J Solid State Electrochem (2011) 15:413–419
DOI 10.1007/s10008-010-1100-2

ORIGINAL PAPER

Effect of oxygen-containing functional groups on the impedance behavior of activated carbon-based electric double-layer capacitors

Ximiao Liu · Yanli Wang · Liang Zhan · Wenming Qiao · Xiaoyi Liang · Licheng Ling

Received: 18 February 2010 / Accepted: 10 May 2010 / Published online: 25 May 2010

Abstract The surface chemistry of activated carbon was treated with sulfuric acid and hydrogen to analyze the oxygen-containing functional groups on the impedance behavior of electric double-layer capacitors. Based on the electrochemical impedance spectrum (EIS), an equivalent circuit model was proposed considering the kinetic and charge transfer characteristics, and Marquardt fit procedure was applied to the EIS data. The simulated results indicate that the oxidation treatment made the ionic resistance within the pore of carbon electrode decrease, and the ion diffusion coefficients significantly increase, which leads to improvement of power capability of the carbon electrode.

Keywords Activated carbon · Electric double-layer capacitor · Impedance · Oxidation

Introduction

Electric double-layer capacitors (EDLCs) are new energy storage devices with great application prospect based on the formation of electric double layer at electrode/electrolyte interface. Compared with rechargeable batteries, EDLCs have many advantages, such as high power density, remarkable cycling performance, high safety, high-temperature stability, friendliness to environment, and so on [1, 2]. During the last decades, EDLCs have been extensively developed [3, 4] to meet the increasing demand in the hybrid power sources for electrical vehicles, digital telecommunication systems, pulse laser techniques, and other energy fields [5, 6].

High surface area activated carbon (HSAC) has been extensively researched as electrode material for EDLCs because of its high specific surface area, excellent electric conductivity, and low cost [7–10]. Recently, considerable efforts have been paid to improve the capacitance by controlling the specific surface area and pore size of HSACs [11–15]. However, these attempts almost approach the capacitance saturation vs. specific surface area at present [16].

Theoretically, the energy density of EDLC is determined by $1/2CV^2$, in which C is the specific capacitance and V is the tolerance voltage [3]. It is a better opinion to obtain a high energy density by improving voltage window rather than specific capacitance. Therefore, focuses of current researches are concentrating on perceiving the reason why there exists tolerance voltage limitation or how to enhance the potential stability. When HSAC was used as electrode material, it should have good electrolyte accessibility except for a high surface area, a good inner pore size, and a high conductivity [17–20]. It has been well known that the oxygen-containing functional groups influence not only the potential of zero charge, the electrolyte wettability of the pores [20], but also the capacitance [21, 22] and inner resistance of EDLCs [18].

In this paper, HSAC was modified by oxidation and deoxidation treatment to give different surface chemical performance. The experiment data of electrochemical impedance were simulated with a new equivalent circuit model considering the kinetic and charge transfer characteristics. The purpose of this work was to investigate the effect of oxygen-containing functional groups on the impedance performance of EDLCs.

X. Liu · Y. Wang · L. Zhan (✉) · W. Qiao · X. Liang · L. Ling
State Key Laboratory of Chemical Engineering, East China University of Science and Technology,
Shanghai 200237, People's Republic of China
e-mail: zhanliang@ecust.edu.cn

Experimental

Materials

HSAC was prepared from petroleum coke with KOH as activation agent [23]. After HSAC was deashed with hydrochloric acid, it was heat-treated at 800 °C for 2 h under hydrogen atmosphere, which was labeled as H-AC. When HSAC was oxidized with sulfuric acid (98 at.%) at 25 °C for 4 h and dried at 220 °C for 2 h under nitrogen atmosphere, it was labeled as O-AC.

EDLC assembly

Polytetrafluoroethylene emulsion with a concentration of 60% was added to the composite electrode materials as binder with a weight ratio of 5% and then kneaded and pressed at 6 MPa to form a round electrode with a diameter of 13 mm and thickness of 0.4 mm. The cells were assembled by stacking two electrodes with a separator, in which nickel foam (100 ppi) and polypropylene porous membrane were used as current collector and separator, respectively. All electrodes were vacuum wetted in 3 M KOH electrolyte before being assembled the simulated EDLCs.

Sample characterization

The pore characteristics of samples were analyzed by nitrogen adsorption at 77 K using an automated apparatus (ASAP 2020M, Micromeritics). The BET surface area (S_{BET}) was analyzed by the Brunauer–Emmett–Teller method. Micropore surface area (S_{mic}) was obtained by the t-plot method using an adsorption branch of isotherm. Total pore size distribution of samples was analyzed with the aid of density functional theory model. The surface chemical compositions of samples were analyzed by X-ray photoelectron spectroscopy (XPS, VG Scientific ESCALab220i-XL).

All the electrochemical experiments were carried out at 25 °C. EDLC cells were charge/discharged for 100 times between 0.05 and 0.9 V at different current densities using an Arbin electrochemical instrument. Specific capacitance was calculated from the slope of the discharge curve by Eq. 1.

$$C = 2I/(m \cdot \mathrm{d}V/\mathrm{d}t) \tag{1}$$

where C is the single-electrode specific capacitance, I the discharge current, m the mass of carbon material in one electrode, and $\mathrm{d}V/\mathrm{d}t$ the slope of the discharge curves. Cyclic voltammetry (CV) measurements were performed at various sweep rates from 5 to 40 mV s^{-1}. Electrochemical impedance spectrum (EIS) was carried out in a frequency range from 10 mHz to 50 kHz with a Gamry electrochemical instrument.

Theory and calculation

The Nyquist plot for a typical experimental double-layer capacitor in the whole frequency range is shown in Fig. 1, which consists of a semicircle at high frequency followed by a 45° inclination and a vertical line at low frequency region. Porosity or roughness of the electrode surface displays a fractal character and is claimed to give rise to the constant phase element (CPE) at high frequency region. The equivalent circuit model to the circuit plot at high frequency region is shown in Fig. 2 where a capacitor is parallel with an interface resistance R_i.

The intercept of the curve with the real axis gives an estimation of the solution resistance R_s. The impedance of a CPE can be determined from Eq. 2

$$Z_{CPE} = 1/\left[Y^0(j\omega)^{\alpha}\right] \tag{2}$$

where j is the imaginary unit $\left(j = \sqrt{-1}\right)$ and ω the angular frequency ($\varpi = 2\pi f$, f being the frequency), α is a dimensionless parameter ranging between 0 and 1 at a solid electrode/solution interface. When Eq. 2 is used to describe an ideal capacitor, the constant $Y^0 = C_i$ (the capacitance) and $\alpha = 1$ [3, 14].

At low frequency region, semi-infinite diffusion can be considered as the rate determining step for a porous electrode. The impedance created by ion diffusion is known as Warburg impedance, which appears as a straight line with a slope of 45° as shown in Fig. 1. The Warburg impedance can be ignored because ions cannot diffuse into the inter pores at high frequencies, whereas ions can diffuse deeper within the porous structure at low frequencies. Therefore, the Nyquist plot becomes a vertical line indicating the pure double-layer capacitive behavior.

If the diffusion layer is totally bounded within a thin slice of solution or a thin slice of material, the Warburg impedance is called the Bounded Warburg (common example for this case is electric double-layer capacitor)

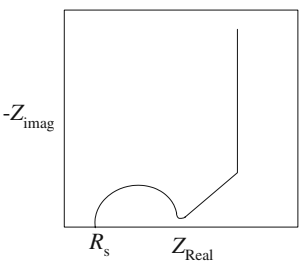

Fig. 1 Experimental Nyquist plot of EDLCs

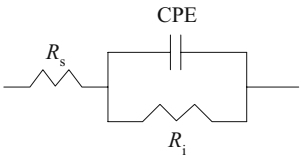

Fig. 2 The equivalent circuit model for the circuit plot at high frequency region

[3, 4]. The impedance of the bounded Warburg is given by:

$$Z_w = Z_0 \Big/ \sqrt{(j\omega)} \coth\left|B\sqrt{j\omega}\right| \quad (3)$$

in which

$$Z_0 = RT \Big/ \left(n^2F^2AC_s\sqrt{D}\right) \quad (4)$$

$$B = \delta \Big/ \sqrt{D} \quad (5)$$

where B and Z_0 are the Warburg factors, D is the diffusion coefficient of the ions in electrolyte, δ is the Nernst diffuse layer thickness, n is the valency of the ion, F is the Faraday constant, A is the area of electrode, and C_s is the concentration of the electrolyte on the surface of electrode. C_s can be replaced by the bulk concentration of the electrolyte because of the reversible formation process of electric double layer.

The above discussion suggests that three parts should be considered when modeling an equivalent circuit corresponding to the capacitor impedance: the electrolyte solution, the interface among carbon particles or/and between particle and current collector, and the ion diffusion within the porous structures. Therefore, considering the kinetic of ion diffusion, a new equivalent circuit model can be described as Fig. 3, and its Nyquist plot is shown in Fig. 1. The whole impedance of the equivalent circuit can be simulated by Eqs. 2 and 3; in detail, Eq. 2 simulates the impedance at high frequency region, and Eq. 3 simulates the impedance at low frequency region.

Results and discussion

Physical properties of carbon electrode materials

Table 1 lists the main pore structure data of different activated carbons. As can be seen, after activated carbon was deoxidated or oxidized, its specific surface area decreased slightly as well as the total pore volume. The pore size distributions (shown in Fig. 4) has no significant change after the treatment.

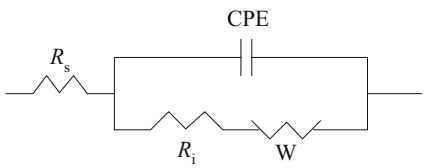

Fig. 3 The equivalent circuit model for the circuit plot at whole frequency range

Table 1 Pore structure data of carbon electrode materials

Samples	S_{BET} (m^2g^{-1})	S_{mic} (m^2g^{-1})	Total pore volume (cm^3g^{-1})	Average pore Size (nm)	Average particle size (μm)
HSAC	2,016	1,980	1.38	2.76	4.8
H-AC	1,956	1,917	1.35	2.72	4.9
O-AC	1,965	1,930	1.36	2.74	4.8

Oxygen-containing functional groups analysis

For a better understanding of surface chemistry by the various treatments, the XPS spectra were deconvolved. The C1s spectra were resolved into four individual component peaks as illustrated in Fig. 5, as follows: peak 1 (284.8 eV), graphitized carbon; peak 2 (286.0±0.2 eV), carbon in phenolic, alcoholic, etheric or C=N groups; peak 3 (287.3±0.2 eV), carbon in carbonyl or quinine groups; and peak 4 (288.8±0.2 eV), carbon in carboxyl or ester groups.

The XPS results are summarized in Table 2. According to the literatures, 80–90% of the peak intensity of the O1s originates from the contribution of the surface atoms or the atoms of the 3.5–4 nm thick outer shell and the C1s peak from C atoms located at the surface or in the 4–5 nm outer shell. As shown in Table 2, the total oxygen content of O-AC sample is much higher than that of HSAC. The phenolic (C–O–) group increase dramatically after treatment with sulfuric acid; the carboxylic groups (O–C=O) decreased from 21.62% to 13.43% after hydrogen treatment, which further leads to the reduction of the total oxygen content.

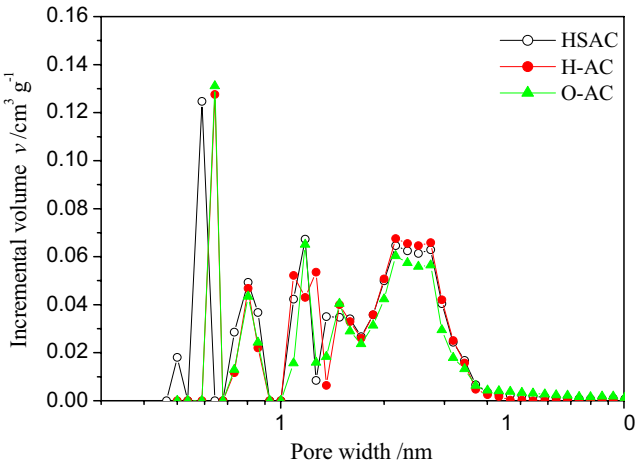

Fig. 4 Pore size distributions of activated carbon samples

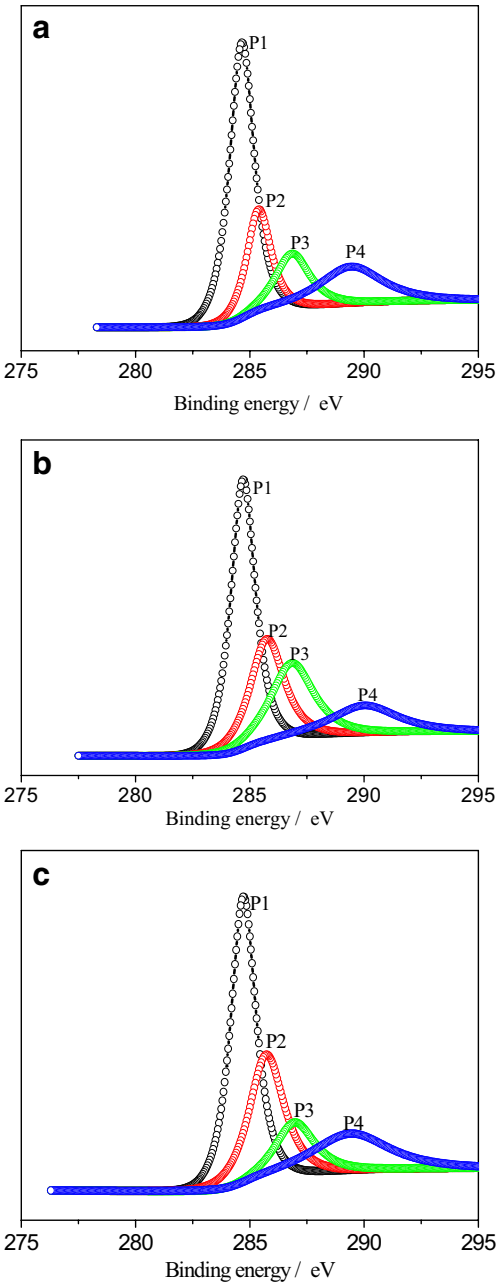

Fig. 5 XPS C1s spectra of activated carbon samples: **a** HSAC, **b** H-AC, and **c** O-AC

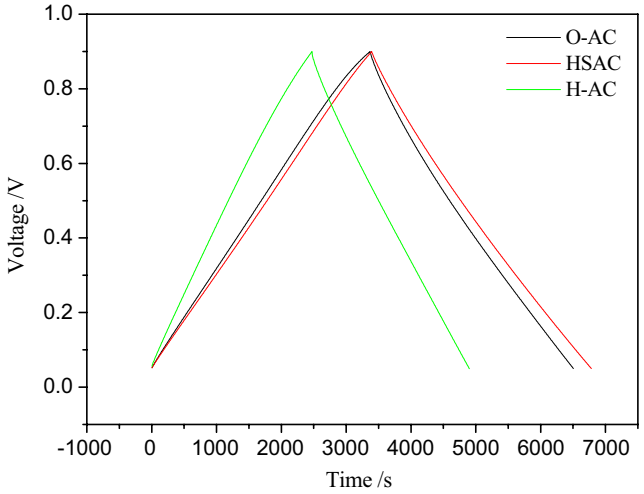

Fig. 6 The charge/discharge curves of the cells with different activated carbons

Electrochemical performance of carbon electrodes

Figure 6 shows the charge/discharge curves of the samples. It is evident that a symmetrical triangle is observable in the range of 0.05–0.9 V at a constant current density of 40 mA g^{-1}. The relationship between specific capacitance and current density was derived from the charge/discharge curves at a current density varying from 40 mA g^{-1} to 8 A g^{-1}. Figure 7 indicates that although the specific capacitance decreased with current density increasing, the specific capacitance of O-AC is the highest, while that of H-AC decreased significantly. The specific capacitance of O-AC was 220 Fg^{-1} at a high current of 8 Ag^{-1}; moreover, it still kept 81.2% of the value measured at 40 mA g^{-1}. Therefore, the oxidation treatment is favorable to improve the capacity of activated carbon, especially at high current density.

Potential sweep CV measurement of the capacitor cells were conducted within 0–0.9 V (shown in Fig. 8a) to analyze the electrochemical behavior of the electrodes. By dividing the induced current with the scan rate and the weight of carbon used, voltammograms of specific capacitance versus potential profiles were obtained, and the results are shown in Fig. 8b. Voltammograms of rectangular shape were observed, indicating the domination of double-layer formation. Although the current or capacitance of the O-AC electrode shows a little deviation from level, the

Table 2 Relative contents of functional groups in C1s from XPS spectra

Samples	C1s (%)				C (at.%)	O (at.%)
	Peak 1	Peak 2	Peak 3	Peak 4		
HSAC	44.83	17.93	15.61	21.62	92.61	7.39
H-AC	49.44	21.14	15.99	13.43	93.94	5.40
O-AC	44.95	26.13	12.26	16.68	86.59	12.43

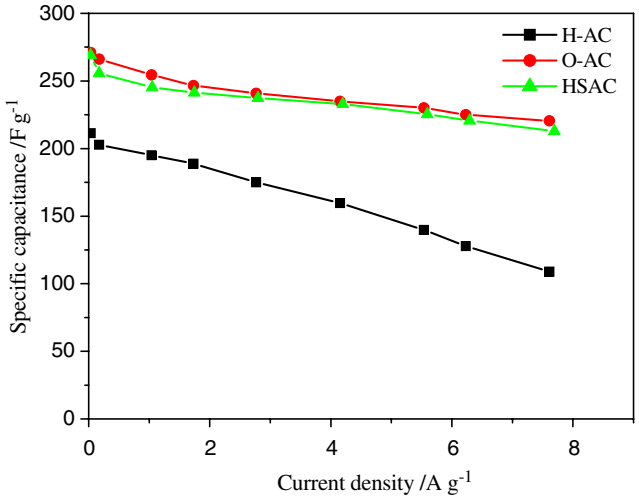

Fig. 7 Relationship between specific capacitance and discharge current density

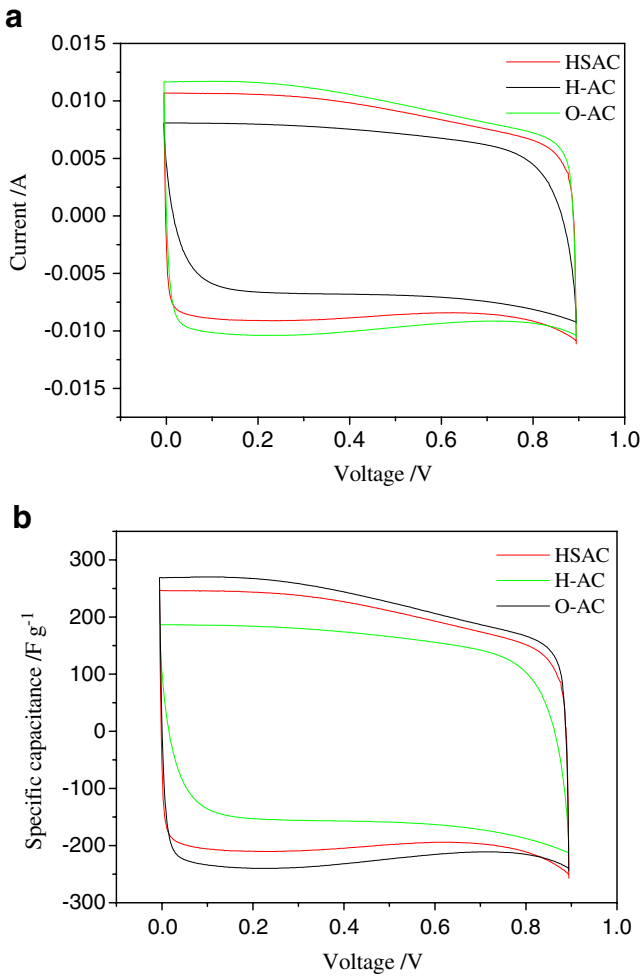

Fig. 8 **a** CV curves of the EDLCs and **b** relationship between specific capacitance and voltage at a sweep rate of 5 mV/s

Faradic current or capacitance peak is not remarkable in the CV curves. Moreover, the specific capacitance of O-AC electrode is higher than that of HSAC, indicating that oxidation treatment can improve the capacitance of activated carbon.

EIS of the modified electrodes

EIS, which distinguishes the resistance and capacitance of devices, was further employed to analyze the performance of the capacitor cells. The impedance spectra of these cells are shown in Fig. 9. It depicts the standard Nyquist plots scans at different potentials. For each sample, there is a semicircle intersecting the real axis at the high frequency region, and the plot transforms to a vertical line with decreasing frequency. Moreover, the simulated curves fit with the EIS data very well. However, the Nyqusit plots present a remarkable difference in the diameter of high frequency semicircle and the length of the line with a slope of 45°. Because the electrochemical process occurring on the exterior surface of the electrodes at high frequencies, the semicircle is suggested to represent the impedance at the interface between the current collector and the carbon particles as well as that among the carbon particles. At the low frequency region, nearly complete ions would be penetrated into pores; the vertical line exhibits the domination of the capacitive behavior at the electrolyte/carbon interface. According to Eqs. 2 and 3, Marquardt fit procedure is applied to EIS data to obtain parameters value, and the results of parameter R_s, R_i, Y^0, α, D, and δ are listed in Table 3.

As can be seen from Table 3, when the concentration of electrolyte remains the same, the values of solution resistance R_s are almost same because it is mainly determined by the electrolyte.

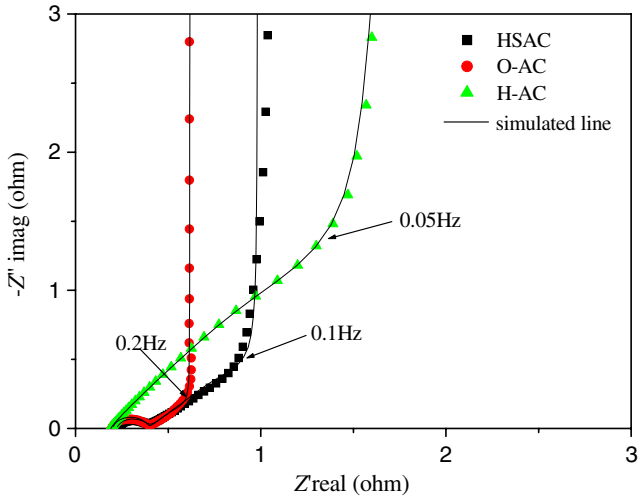

Fig. 9 The experimental and simulated Nyquist plots of EDLCs

Table 3 Parameter data simulated with Eqs. 2 and 3

Parameters	Results of samples		
	HSAC	H-AC	O-AC
R_s (mΩ)	222.8	190.8	200.1
R_i (mΩ)	168	77.89	191.1
$Y^0\times10^3$ ($\Omega^{-1}s^{1/2}$)	1.42	2.41	8.43
α	860	810	887
$D\times10^9$ (cm^2s^{-1})	8.34	1.64	22.0
$\delta\times10^4$ (cm)	2.36	1.31	2.27
R_Ω (mΩ)	619	1,740	226

The value of R_i for the cell with H-AC as electrode material is the lowest, and it follows the order: H-AC< HSAC<O-AC. These indicate that the polarization resistance of the cells increases with the amount of surface oxides increasing.

The exponent α deviates from unity and increases with the amount of oxygen-containing functional groups, indicating that the external surface becomes more ideal because such surface functional groups may improve the surface hydrophilicity of activated carbon and be more wettable with electrolyte.

The constant Y^0 is too small to be taken into account in evaluating the external surface capacitance due to the fact that CPE represents the external surface of carbon.

The inner pore diffusion coefficient D increases remarkably with the oxygen-containing functional groups increasing. This may be attributed to the fact that oxygen-containing functional groups improve the surface hydrophilicity and wettability with electrolyte, which leads to a higher inner-pore ion diffusion rate. The increase in diffusion coefficient accordingly causes the internal resistance R_Ω to decrease. In addition, the values of R_Ω are much higher than that of R_i, indicating that the overall resistance of the EDLCs is controlled by the inner-pore diffusion coefficient.

The values of parameter δ are quite low and have no obvious change, which suggests that the concentration polarization is not remarkable.

As a result of a resistance within the pore structure, non-uniform charge distribution through the porous electrode at high charging rates or at high frequencies exists, leading to a distributed capacitance effect, which can be derived from the impedance spectra (Fig. 9). The relationships between capacitance and frequency are shown in Fig. 10. The capacitance can be calculated from the imaginary part of the impedance as follows:

$$Z_{imag} = C^{-1}\varpi^{-1} \quad (6)$$

where Z_{imag}, C, and ω are the imaginary components of the impedance, capacitance, and the angular velocity, respectively.

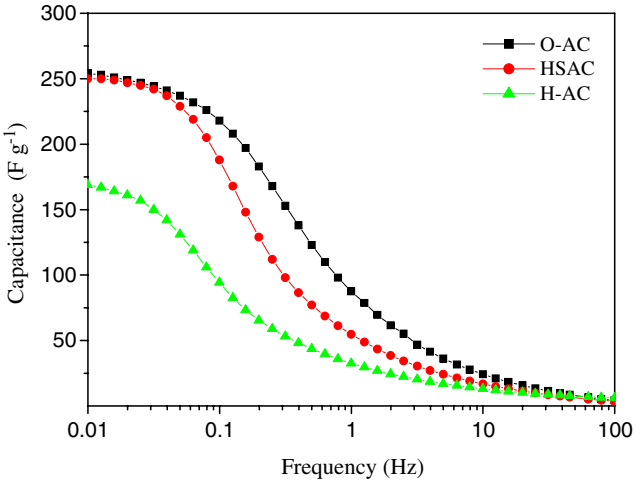

Fig. 10 Relationship between capacitance and frequency for different carbon electrodes

As seen from Fig. 10, the capacitance increases with frequency decreasing in an inverse S-shaped mode. The capacitance levels off at lower frequency and starts to decrease abruptly at high frequency. The cut-off frequency is roughly related to the RC time constant of the single electrode capacitor. For the cell with O-AC, the low frequency capacitance is higher than others. However, its RC time constant is lower, which is reflected by the higher cut-off frequency. This can be mainly attributed to the lower ion diffusion resistance of O-AC. Moreover, the RC time constant follows the order of H-AC>HSAC>O-AC. The results indicate that the introduction of oxide group on the activated carbon surface would improve the power capability of EDLCs.

Conclusions

In this work, the effects of oxygen-containing functional groups of activated carbon on the electrochemical performance of carbon electrode were investigated using an impendence method and relating model. The results indicate that oxygen-containing functional groups of activated carbon lead to a significant increase of inner-pore ion diffusion coefficient and a decrease in ionic resistance within the pore of carbon electrode. Although oxide groups cause polarization resistance of the electrode increase, the overall inner resistance of the cell is dominated by the inner-pore ionic resistance. Therefore, oxidation treatment may improve the power capability of activated carbon.

Acknowledgments This work was supported by the National Science Foundation of China (nos. 50730003, 50672025, and

20806024) and the Research Fund of China for the Doctoral Program of Higher Education (no. 20070251008).

References

1. He XJ, Lei JW, Geng YJ, Zhang XY, Wu MB, Zheng MD (2009) J Phys Chem Solids 70:738–744
2. Balathanigaimani MS, Shim WG, Lee MJ, Kim C, Lee JW, Moon H (2008) Electrochem Commun 10:868–871
3. Conway BE (1999) Electrochemical supercapacitors—scientific fundamentals and technological applications. Kluwer, New York
4. Kótz R, Carlen MJ (2000) Electrochim Acta 45:2483–2498
5. Castelló DL, Amorós DC, Solano AL, Shiraishi S, Kurihara H, Oya AJ (2003) Carbon 41:1765–1775
6. Kim IJ, Yang SY, Jeon M, Moon SI, Kim HS, Lee YP, An KH, Lee YH (2007) J Power Sources 173:621–625
7. Gamby J, Taberna PL, Simon P, Fauvarque JF, Chesneau MJ (2001) J Power Sources 101:109–116
8. Pell WG, Conway BE, Marincic NJ (2000) J Electroanal Chem 491:9–13
9. Qu DYJ (2002) J Power Sources 109:403–411
10. Hu CC, Wang CC, Wu FC, Tseng RL (2007) Electrochim Acta 52:2498–2505
11. Yoon S, Jang JH, Ka BH, Oh SMJ (2005) Electrochim Acta 50:2255–2262
12. Huang CW, Chuang CM, Ting JM, Teng HS (2008) J Power Sources 183:406–410
13. Show YSYK, Imaizumi K (2006) Diamond Relat Mater 15:2086–2089
14. Zoltowski P (1998) J Electroanal Chem 443:149–154
15. Tóth S, Füle M, Veres M, Selman JR, Arcon D, Pócsik I, Koós MJ (2005) Thin Solid Films 482:207–210
16. Qu DY, Shi HJ (1998) J Power Sources 74:99–107
17. Toupin M, Bélanger D, Hill IR, Quinn DJ (2005) J Power Sources 140:203–210
18. Nian YR, Teng HJ (2003) J Electroanal Chem 540:119–127
19. Portet C, Taberna PL, Simon P, Robert CLJ (2004) Electrochim Acta 49:905–912
20. Xu B, Wu F, Chen S, Zhang CZ, Cao GP, Yang YS (2007) Electrochim Acta 52:4595–5498
21. Hsieh CT, Teng H (2002) Carbon 40:667–674
22. Martínez MJB, Agulló JAM, Castelló DL, Morallón E (2005) Carbon 43:2677–2684
23. Liu XM, Zhan L, Teng N, Yang DL, Zeng XC, Zhang R, Ling LC (2006) New Carbon Mater 21:48–53